

# Transferability Estimation Based On Principal Gradient Expectation

Huiyan Qi  
Fudan University

huiyanqi21@m.fudan.edu.cn

Lechao Cheng  
Zhejiang Lab

chenglcl@zhejianglab.com

Jingjing Chen  
Fudan University

chenjingjing@fudan.edu.cn

Yue Yu  
Fudan University  
yu.y21@m.fudan.edu.cn

Zunlei Feng  
Zhejiang University  
zunleifeng@zju.edu.cn

YuGang Jiang  
Fudan University  
yggj@fudan.edu.cn

## Abstract

Deep transfer learning has been widely used for knowledge transmission in recent years. The standard approach of pre-training and subsequently fine-tuning, or linear probing [4], has shown itself to be effective in many downstream tasks. Therefore, a challenging and ongoing question arises: how to quantify cross-task transferability that is compatible with transferred results while keeping self-consistency? Existing transferability metrics are estimated on the particular model by conversing source and target tasks. They must be recalculated with all existing source tasks whenever a novel unknown target task is encountered, which is extremely computationally expensive. In this work, we highlight what properties should be satisfied and evaluate existing metrics in light of these characteristics. Building upon this, we propose Principal Gradient Expectation (PGE), a simple yet effective method for assessing transferability across tasks. Specifically, we use a restart scheme to calculate every batch gradient over each weight unit more than once, and then we take the average of all the gradients to get the expectation. Thus, the transferability between the source and target task is estimated by computing the distance of normalized principal gradients. Extensive experiments show that the proposed transferability metric is more stable, reliable and efficient than SOTA methods.

## 1. Introduction

With the advance of deep learning approaches, an increasing number of models with enormous capacity paired with large-scale datasets have demonstrated superior performance in many applications. However, the majority of these models are tailored to particular tasks, resulting in limited transferability. Thus, a surge of interest emerges in transferring knowledge from the source task into the target task based on pre-training mechanism [34, 35]. In the

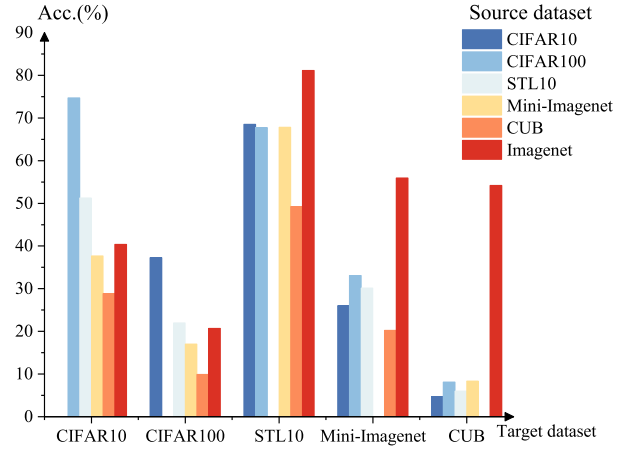


Figure 1. Using the architecture of Resnet18, the horizontal coordinates in the figure indicate the target dataset, the different color legends indicate different source datasets which used to train the model. Fix the feature extractor part of the model and train the classifier on the target dataset.

realm of computer vision, the prevalent adaptations of pre-trained models are mainly fine-tuning and linear probing. Fine-tuning approaches adapt the entire parameters of the backbone for the target task, while linear probing always adapts the model outputs by learning a task-related head layer. Both of the fine-tuning/linear probing [4] leverage models pre-trained on large-scale general datasets to adapt to specific downstream tasks.

Prominent models, including BERT [8] and GPT-3 [3] for natural language processing, the ResNet [14] and vision transformer [11, 20, 21] variants pre-trained on ImageNet [31] for vision tasks, and the CLIP [28, 29, 32] variants for multimodal learning, have significantly outperformed previous approaches in their fields of expertise and achieved state-of-the-art results in a variety of downstream

tasks.

The orthodoxy encourages us that the big capacity of the model together with the larger amount of data, facilitates the performance of downstream tasks. However, we find that this intuitive assumption does not hold in real scenarios, as illustrated in Figure 1. We conduct toy experiments to validate pre-training transmission between different datasets (CIFAR10 [18], CIFAR100 [18], STL10 [5], Mini-ImageNet [40], and Caltech-USCD Birds 2011(CUB) [41]) under the same backbone (ResNet18). The experimental results reveal that utilizing pre-training backbones on larger datasets may not always yield the optimal outcomes for all target datasets, as also empirically demonstrated in [1]. For example, the most suitable pre-trained model for CIFAR10 [18] is CIFAR100 [18], and vice versa. For more challenging target datasets (STL10 [5], Mini-ImageNet [40], and CUB [41]), the parameters pretrained on ImageNet [31] are more effective. These observations motivate us to investigate how to identify the best pre-trained models for downstream tasks.

To address the aforementioned issues, researchers have proposed several transferability metrics, including LEEP [24], LogMe [44], H-score [2], NCE [39], GBC [26]. However, these solutions confront with two significant challenges: inadequate complexity and less trustworthiness. Most above methods are extremely computationally expensive for the reason that the transferability scores are calculated by conversing source and target tasks, and they must be recalculated with all existing source tasks whenever a novel unknown target task is encountered. In addition, transferability ratings of existing approaches are only marginally positive / correlated with the transferred accuracy of multiple source task for the challenging target task.

When delving deeper into the problem, we believe two essential concepts must be specified before developing a transferability measurement. The first is about properly assessing the causality between transferability ratings and actual transfer results. The second concern is what properties a good transferability estimation should possess. In this paper, for the first time, we investigate these two concepts and introduce a transferability estimation approach based on principal gradient expectation. First, we undertake robust evaluation by repeatedly selecting sub-datasets of varying proportions to mitigate the disruption of a single transfer result, as described in Section 3.3. Then, we consider that a good transferability measurement should be stable, distinguishable, efficient, and irrelevant to the task. Based on these presumptions, we suggest a straightforward yet effective technique for transferability estimation that exhibits these characteristics, dubbed Principal Gradient Expectation (PGE). Specifically, PGE collects first-order gradients per-batch and empirically average the gradients to form principal gradients. Notably, the first-order gradient is com-

puted using the backbone in unsupervised mode, such as few-shot or contrast learning. It has been experimentally found [16, 45] that supervised pretraining is more susceptible than unsupervised pretraining because category information may be embedded into the network to improve discrimination while obstructing transferability. Then, we relax the distance of the principal gradient expectation between the source and target tasks by Schwarz inequality [36] to achieve a lower bound as the quantitative transferability score. In light of the fact that earlier research may have focused more on the situation of linear probing, we examine both fine-tuning and linear probing comprehensively and the experimental results exhibit superior properties to those of earlier approaches. To limit the impact of other variables on our studies, we choose ResNet as the standard backbone. Extensive experimental results on different datasets indicate that our strategy is more applicable to real transfer scenery.

To conclude, the main contributions of this work can be summarized as follows:

- For the first time, we suggest that a qualified transferability metric should be stable, reliable and efficient.
- We introduce a novel approach based on the principal gradient expectation for assessing transferability. Our method favors the above properties, which shows its superiority to other methods.
- We show through experiments that the proposed PGE is strongly related to the transferred results. Our approach is simple yet effective that doesn't require a complicated optimization process.

## 2. Related Work

Our work relates to transfer learning [38], pre-training methods, and transferability estimation [37]. We next discuss related work in these four domains that are closely related to our work.

### 2.1. Transfer Learning

Transfer learning aims to acquire knowledge of the source domain and the source task to help learn the prediction results for the target domain. In addition to using different pre-training models for transfer learning, there are many fine-tuning techniques, such as Li *et al.* [43] studied the effect of different regularization schemes on transfer results. Kumar *et al.* [19] improved the transfer effect by first freezing the parameters of the feature extractor and then fine-tuning the whole model. Wei *et al.* [42] recently addressed the problem of multi-source transfer by modeling the correlation between domains. Renggli *et al.* [30]

searched for better source models with a hybrid search strategy, which relies on the performance of ImageNet on different models. Often, the pre-trained parameters are trained on large-scale datasets, but this does not always favor downstream tasks. The suggestion in [17] that using regularization to improve the accuracy of ImageNet pre-training can compromise the accuracy of downstream tasks yields similar conclusions as [1].

## 2.2. Pre-Training

ImageNet is the most commonly used dataset for pre-training, and the standard pre-training method is to perform supervised pre-training. When using convolutional neural networks for image classification tasks, Djolonga *et al.* [10] discovered that increasing the training set and model size can improve the robustness of distribution shifts. Recently, there has been extensive interest in pre-training with unsupervised or self-supervised methods that fully use unlabeled data. For models pre-trained using large-scale datasets, Abnar *et al.* [1] found that as the upstream task accuracy increases, the performance of the downstream task saturates, so to get better downstream performance, we can try to compromise the upstream task accuracy. With the development of pre-training using unsupervised and self-supervised approaches, Zhao *et al.* [45] and Islam *et al.* [16] verified the importance of mid-level and low-level representations, where pre-training using unsupervised or self-supervised approaches would improve the transferability. In contrast, supervised approaches would weaken the transferability.

## 2.3. Transferability Estimation

To properly evaluate the transferability of pre-trained models, Negative Conditional Entropy (NCE) [39] utilizes a metric derived from information theory to measure the transferability and difficulty of classification tasks. NCE assumes that the images of a source task and a target task are the same, but their labels are distinct. They then use the negative conditional entropy between the target and the source labels as a transferability measure. Contemporary work h-score [2] also leverages statistics and information theory to quantify the transferability of feature representations across tasks. However, h-score can only be employed in classification problems. While LEEP [24] focuses on computing the joint probability over pre-trained labels and the target labels to yield log expectation of the empirical predictor. But when source models with identical feature extractors and distinct classification heads will generate different transferability scores. LogMe [44] alleviates this issue by directly estimating the maximum value of label evidence given features extracted by pre-trained models. It models each target label as a linear model with Gaussian noise, and then optimizes the prior distribution parameters to obtain the average maximum (log) evidence of labels given the target sam-

ple embeddings. Recently, GBC [26] desires to measure the amount of overlap between target classes in the feature space of the source model. While in this work, we employed the gradients of the model’s backbone in our estimations, assuring the precision of our technique.

## 3. Method

Regarding a model  $\mathcal{M}(w, h)$  and a task  $\mathcal{T}$ , we denote the feature extractor part of the model by  $w$  and the task-related layer by  $h$ . Given  $N$  alternative source datasets  $\{\mathcal{D}_i\}_{i=1}^N$  and a target dataset  $\mathcal{D}_t$ , our goal is to quantify and estimate the transferability between each source dataset  $\mathcal{D}_s^i$  and  $\mathcal{D}_t$  to determine the appropriate source dataset for that target dataset  $\mathcal{D}_t$ . The selection process is critical for the efficiency of transfer learning. We use  $\mathcal{S}(\mathcal{D}_s, \mathcal{D}_t; \mathcal{T})$  to denote the transferability estimation from  $\mathcal{D}_s$  to  $\mathcal{D}_t$ .

By analyzing the previous methods, we summarize three characteristics of an excellent transferability metric: stability, reliability, and efficiency. Next, we give a detailed description of these three definitions.

**Definition 1(Stability)** Given  $\mathcal{D}_s$ ,  $\mathcal{D}_t$  and a subset of  $\mathcal{D}_t^i \subset \mathcal{D}_t$ , the stability is that the difference between the two transferability metric values  $\mathcal{S}(\mathcal{D}_s, \mathcal{D}_t^i; \mathcal{T})$  and  $\mathcal{S}(\mathcal{D}_s, \mathcal{D}_t; \mathcal{T})$  is bounded, which can be described as:

$$|\mathcal{S}(\mathcal{D}_s, \mathcal{D}_t^i; \mathcal{T}) - \mathcal{S}(\mathcal{D}_s, \mathcal{D}_t; \mathcal{T})| \leq \epsilon. \quad (1)$$

Stability is essential since a finite dataset itself is a subsample in the manifold space of the data distribution.

**Definition 2(Reliability)** We define  $\mathcal{A}(\mathcal{D}_s^i, \mathcal{D}_t)$  as the result transferred from  $\mathcal{D}_s^i$  to the  $\mathcal{D}_t$ .  $\mathcal{S}(\mathcal{D}_s^i, \mathcal{D}_t)$  is the transferability distance score. Thus,  $\mathcal{S}(\mathcal{D}_s^i, \mathcal{D}_t; \mathcal{T}) < \mathcal{S}(\mathcal{D}_s^j, \mathcal{D}_t; \mathcal{T})$  always enables:

$$\mathcal{A}(\mathcal{D}_s^i, \mathcal{D}_t; \mathcal{T}) > \mathcal{A}(\mathcal{D}_s^j, \mathcal{D}_t; \mathcal{T}). \quad (2)$$

In practical, the Kendall’s coefficient or correlation coefficient are often employed to quantify the matched ranking. More details can be found in Section 4.

**Definition 3(Efficiency)** The estimation of the transferability from source to target dataset is supposed to be quick and simple.

Previous works [45] and [16] demonstrated that the transferability is mainly related to low-level and mid-level features. The label space of the data also affects the transferability. We only used the gradient of the backbone part  $w$  of the model in our calculation, ensuring our method’s accuracy. We do not need to train all the source domains in the computation as other methods do. In short, our process does not require pre-training. To ensure the stability of the results, we use the expectation of the principal gradient in our computation, which reduces the impact of the outliers in this way. Next, we describe our method.

### 3.1. Fast Approximation of Model Similarity

Given a model  $\mathcal{M}$ , a dataset  $\mathcal{D}$  and a learning task  $\mathcal{T}$ . The dataset is divided into many batches. The batches are denoted as  $\{\mathcal{B}_i\}_{i=1}^M$ , where  $M$  is the number of batches.  $\mathcal{L}_D$  is the loss function of model  $\mathcal{M}$  on the dataset  $\mathcal{D}$ . Minimizing the Loss  $\mathcal{L}_D$  is the optimization objective on the dataset  $\mathcal{D}$ .

We need to calculate the gradient of model parameters on every batch. The model is initialized with weights  $\theta_0$  which is the starting point of the optimization. The initialized weights  $\theta_0$  are sampled from a distribution  $\mathcal{N}(\mathbf{0}, I)$ . Multi-sampling increases the stability of the calculation. The loss of a batch  $\mathcal{B}_i$  at the starting point  $\theta_0$  is denoted as  $\mathcal{L}_D(\mathcal{B}_i, \theta_0)$ , and its gradient is denoted as  $\nabla \mathcal{L}_D(\mathcal{B}_i, \theta_0)$ . We re-initialized the weights for the next batch  $\mathcal{B}_{i+1}$ .

In contrast with gradient descent, we do not use the gradient to update the weights. We compute the expectation of different batches' gradients at the starting point  $\theta_0$ . This expectation is defined as Principal Gradient Expectation (PGE) for dataset  $\mathcal{D}$ , which can be described as:

$$PGE_D = \mathbb{E}_{i, \theta_0} [\nabla \mathcal{L}_D(\mathcal{B}_i, \theta_0)]. \quad (3)$$

With the definition of PGE, we compute the PGE for source dataset  $\mathcal{D}_s$  and target dataset  $\mathcal{D}_t$  respectively with their own loss functions  $\mathcal{L}_{D_s}$  and  $\mathcal{L}_{D_t}$ :

$$PGE_{D_s} = \mathbb{E}_{i, \theta_0} [\nabla \mathcal{L}_{D_s}(\mathcal{B}_i, \theta_0)], \quad (4)$$

$$PGE_{D_t} = \mathbb{E}_{i, \theta_0} [\nabla \mathcal{L}_{D_t}(\mathcal{B}_i, \theta_0)]. \quad (5)$$

### 3.2. Transferability Metric based on Principal Gradient Expectation

Throughout the computation, the label space of the  $\mathcal{D}$  is not used, assuming  $\mathcal{M}(w, h)$ , inputting  $x \in \mathcal{X}$  into  $w$  to obtain the feature representation  $r$  of  $x$ ,  $r = w(x)$ , and  $h$  is the task-relevant layer, where the input to  $h$  is  $r$ , returning the probability distribution. In computing the PGE, we only collect the gradients of  $w$ , making the method more tasks irrelevant. Suppose  $\theta^*$  is the optimal point of the model parameters when training a domain using  $M$ , and  $\theta_0$  is a random initialized parameter. We use  $\theta_s^*$  and  $\theta_t^*$  to denote the optimal points of the source domain and target domain, respectively. The loss function at  $\theta^*$  could be extended in the following form:

$$\mathcal{L}_D(\theta^*) = \mathcal{L}_D(\theta_0) + \nabla \mathcal{L}_D(\theta_0)(\theta^* - \theta_0) + R_2(\theta_0). \quad (6)$$

As shown in Eq.6,  $\nabla \mathcal{L}(\theta_0)$  can be seen as the first-order partial derivative of  $\mathcal{L}$  at point  $\theta_0$ , where  $(\theta^* - \theta_0)$  is the distance between  $\theta^*$  and  $\theta_0$ . We change the order of Eq.6 to obtain Eq.7:

$$(\theta^* - \theta_0) + R_2(\theta_0) = \frac{\mathcal{L}_D(\theta^*) - \mathcal{L}_D(\theta_0)}{\nabla \mathcal{L}_D(\theta_0)}. \quad (7)$$

Eq.7 indicates that the distance between  $\theta^*$  and  $\theta_0$  has proportional to  $1/\nabla \mathcal{L}_D(\theta_0)$ .

As most of pre-trained models are trained via pretext task or classification task with cross-entropy loss, it is reasonable for us to make a strong assumption  $\mathcal{L}(\theta^*) = 0$ , where  $\theta^*$  is the optimal point of the optimization. In Equation 6, let  $\mathcal{L}(\theta^*) = 0$  and ignore the remainder  $R_2(\theta_0)$ . The remaining item is defined as  $\text{dist}(\theta_s^*, \theta_0)$  to represent the distance between  $\theta_s^*$  and  $\theta_0$ . Finally, we get Eq.8.

$$\frac{\mathcal{L}(\theta_0)}{\nabla \mathcal{L}_D(\theta_0)} = \text{dist}(\theta_s^*, \theta_0). \quad (8)$$

For both  $\mathcal{D}_s$  and  $\mathcal{D}_t$ , we can use the expression of Equation 9, as shown in Eq.9 and Eq.10.

$$\frac{\mathcal{L}(\theta_0)}{\nabla \mathcal{L}_{D_s}(\theta_0)} = \text{dist}(\theta_s^*, \theta_0). \quad (9)$$

$$\frac{\mathcal{L}(\theta_0)}{\nabla \mathcal{L}_{D_t}(\theta_0)} = \text{dist}(\theta_t^*, \theta_0). \quad (10)$$

Subtract Eq.9 and Eq.10 left and right, respectively, and we get Eq.11.

$$\mathcal{L}(\theta_0) \left( \frac{1}{\nabla \mathcal{L}_{D_t}(\theta_0)} - \frac{1}{\nabla \mathcal{L}_{D_s}(\theta_0)} \right) = \text{dist}(\theta_s^*, \theta_0). \quad (11)$$

As shown in Eq.11, the left-hand side is rewritten to use the  $l_2$  norm.

$$\mathcal{L}(\theta_0) \left\| \frac{1}{\nabla \mathcal{L}_{D_t}(\theta_0)} - \frac{1}{\nabla \mathcal{L}_{D_s}(\theta_0)} \right\|_2 = \mathcal{S}(\mathcal{D}_s, \mathcal{D}_t; \mathcal{T}). \quad (12)$$

Considering that  $\nabla \mathcal{L}_D(\theta_0)$  may be small, this leads to possible anomalies in the result when solving for  $1/\nabla \mathcal{L}_{D_t}(\theta_0)$ . It affects the stability of our results, so we use Schwarz inequality [36] to deflate  $1/\nabla \mathcal{L}_{D_t}(\theta_0) - 1/\nabla \mathcal{L}_{D_s}(\theta_0)$ .

$$\left\| \frac{1}{\nabla \mathcal{L}_{D_t}(\theta_0)} - \frac{1}{\nabla \mathcal{L}_{D_s}(\theta_0)} \right\|_2 \geq \frac{\| \nabla \mathcal{L}_{D_t}(\theta_0) - \nabla \mathcal{L}_{D_s}(\theta_0) \|_2}{\| \nabla \mathcal{L}_{D_t}(\theta_0) \|_2 \| \nabla \mathcal{L}_{D_s}(\theta_0) \|_2}. \quad (13)$$

We define the formula to calculate the transferability score as follows:

$$\begin{aligned} \mathcal{S}(\mathcal{D}_s, \mathcal{D}_t; \mathcal{T}) &= \frac{\| PGE_{D_t} - PGE_{D_s} \|_2}{\| PGE_{D_t} \|_2 \| PGE_{D_s} \|_2} \\ &= \frac{\| \mathbb{E}_{i, \theta_0} [\nabla \mathcal{L}_{D_t}(\theta_0)] - \mathbb{E}_{i, \theta_0} [\nabla \mathcal{L}_{D_s}(\theta_0)] \|_2}{\| \mathbb{E}_{i, \theta_0} [\nabla \mathcal{L}_{D_t}(\theta_0)] \|_2 \| \mathbb{E}_{i, \theta_0} [\nabla \mathcal{L}_{D_s}(\theta_0)] \|_2}. \end{aligned} \quad (14)$$

In the actual calculation, we only use the gradient of  $w$  of  $\mathcal{M}$ . Intuitively, this metric tells us the difference in gradient



between  $\mathcal{D}_s$  and  $\mathcal{D}_t$ . We believe the  $\mathbb{E}_{i,\theta_0} [\nabla \mathcal{L}_D(\theta_0)]$  reflects the optimization direction of the domain, which points to the optimal point. It can be used to measure the distance between the two optimal points of  $\mathcal{D}_s$  and  $\mathcal{D}_t$ , so the score obtained in this way can be used as a metric of transferability. Then we can calculate and rank the transferability score between each  $\mathcal{D}_s^i$  in  $\{\mathcal{D}_s^n\}_{n=1}^N$  and  $\mathcal{D}_t$ .

The algorithm for obtaining the mixability score using PGE is described in Algorithm 1.

---

**Algorithm 1** Principal Gradient Expectation

---

**Input:** A model  $\mathcal{M}$  with random initialization, several different source datasets  $\{\mathcal{D}_s^n\}_{n=1}^N$ , and target dataset  $\mathcal{D}_t$ .

**Output:** Ranking of the results of transfer of all source datasets to target datasets when using  $\mathcal{M}$ .

$I = \text{epochs} * \text{len}(\text{data loader})$  //  $I$  denotes the number of iterations

**for**  $n = 1 \rightarrow N + 1$  **do** //  $N + 1$  denotes  $N$  sources and a target

**for**  $i = 1 \rightarrow I$  **do**

        Input a sample set  $B_i, B_i \in \mathcal{D}_s^i$  or  $\mathcal{D}_t$ .

        Computing  $\nabla \mathcal{L}_D(B_i, \theta_0)$

$\mathbb{E}_{i,\theta_0} [\nabla \mathcal{L}_D(B_i, \theta_0)] \leftarrow ((i - 1) * \mathbb{E}_{i,\theta_0} [\nabla \mathcal{L}_D(B_i, \theta_0)] + \nabla \mathcal{L}_D(B_i, \theta_0)) / i$  // The gradients obtained this time are added to the previously collected gradients and averaged

**end for**

**end for**

**for**  $i = 1 \rightarrow N$  **do** //  $N$  denotes the number of sources

    Calculate  $\frac{\|\mathbb{E}_{i,\theta_0} [\nabla \mathcal{L}_{D_t}(\theta_0)] - \mathbb{E}_{i,\theta_0} [\nabla \mathcal{L}_{D_s}(\theta_0)]\|_2}{\|\mathbb{E}_{i,\theta_0} [\nabla \mathcal{L}_{D_t}(\theta_0)]\|_2 \|\mathbb{E}_{i,\theta_0} [\nabla \mathcal{L}_{D_s}(\theta_0)]\|_2}$

**end for**

Sort

**return** Ranking

---

### 3.3. Robust Evaluation with Multiple Subsampling

In this section, we introduce the standardized evaluation for the transferability between different datasets.

If  $\mathcal{A}(\mathcal{D}_s^i, \mathcal{D}_t; \mathcal{T}) > \mathcal{A}(\mathcal{D}_s^j, \mathcal{D}_t; \mathcal{T})$ , we expect  $\mathcal{S}(\mathcal{D}_s^i, \mathcal{D}_t; \mathcal{T}) < \mathcal{S}(\mathcal{D}_s^j, \mathcal{D}_t; \mathcal{T})$ .  $\{\mathcal{A}(\mathcal{D}_s^i, \mathcal{D}_t)\}_{i=1}^N$  denotes the set of results of transferring of the  $\mathcal{D}_s^i$  to the  $\mathcal{D}_t$ .  $\{\mathcal{S}(\mathcal{D}_s^i, \mathcal{D}_t)\}_{i=1}^N$  denotes the set of scores between the  $\mathcal{D}_s^i$  to the  $\mathcal{D}_t$ . Kendall's  $\tau$  [13] coefficient captures this well. So we use it to measure the method's effectiveness for computing the transferability metric score. The range of values of  $\tau$  is  $[-1, 1]$ , a larger  $\tau$  means a higher correlation between  $\{\mathcal{A}(\mathcal{D}_s^i, \mathcal{D}_t; \mathcal{T})\}_{i=1}^N$  and  $\{\mathcal{S}(\mathcal{D}_s^i, \mathcal{D}_t; \mathcal{T})\}_{i=1}^N$ . When  $\tau = 0$  shows no correlation. This approach was applied to measure the accuracy of the transferability metric.

To measure the stability of the metric, we generate multiple subsets of the target dataset  $\mathcal{D}_t$  with two approaches:

(1) Randomly pick a percentage  $\eta_1$ .  $\eta_1$  of all categories are randomly selected, but all samples in the chosen categories are used. (2) Randomly pick a percentage  $\eta_2$ . All categories are used, but only  $\eta_2$  samples of each category was randomly selected. In the transfer experiment, we fine-tuned the pre-trained model, which is trained on  $\mathcal{D}_s$ , with different subsets of  $\mathcal{D}_t$ . Multiple adapted models are obtained with different sampling parameters  $\eta_1$  or  $\eta_2$ . A curve is drawn on how the parameters  $\eta_1$  or  $\eta_2$  affect the performance of the adapted models. The horizontal axis represents  $\eta_1$  or  $\eta_2$  which indicate the sizes of the subsets. The vertical axis shows the performance of the adapted models, e.g. accuracy for the classification task. We use the area under the curve as the measurement of the transferability from  $\mathcal{D}_s^i$  to  $\mathcal{D}_t$ . The area is denoted as  $\mathcal{A}(\mathcal{D}_s^i, \mathcal{D}_t; \mathcal{T})$ . We measure the stability of the method using the correspondence between the transfer results and the transferability scores of the sub-target datasets.

## 4. Experiment

In this section, we investigate and validate the proposed transferability metric using real-world image data. We first introduce the basic experimental settings and then evaluate the proposed PGE from four aspects: stability, reliability, efficiency, and generalizability.

### 4.1. Experimental Settings

**Dataset.** Our experiments are conducted on the following classification datasets: CIFAR10 [18], CIFAR100 [18], STL10 [5], Mini-ImageNet [40], CUB [41], MNIST [7], FGVC-Aircraft (Aircraft) [23]. To validate the effectiveness of cross-task transfer, we adopt PASCAL VOC 2012 [12] for the target dataset. The information, including the resolution size (Resolution), image number (Img), and class number (Class) of above datasets are summarized in Table 1.

Dataset	Resolution	Img	Class
CIFAR10 [18]	$32 \times 32$	60k	10
CIFAR100 [18]	$32 \times 32$	60k	100
STL10 [5]	$96 \times 96$	13k	10
Mini-ImageNet [40]	$84 \times 84$	60k	200
CUB [41]	$512 \times 512$	11.7k	200
MNIST [7]	$28 \times 28$	70k	10
Aircraft [23]	$512 \times 512$	10k	100
PASCAL VOC 2012 [12]	$320 \times 480$	1.7k	21

Table 1. The summary information of datasets used in this work.

**Evaluation.** We construct the evaluation sub-datasets by two approaches as follows:

**SI:** The first approach randomly samples 5% to 100% of the target categories and uses all images in these categories.

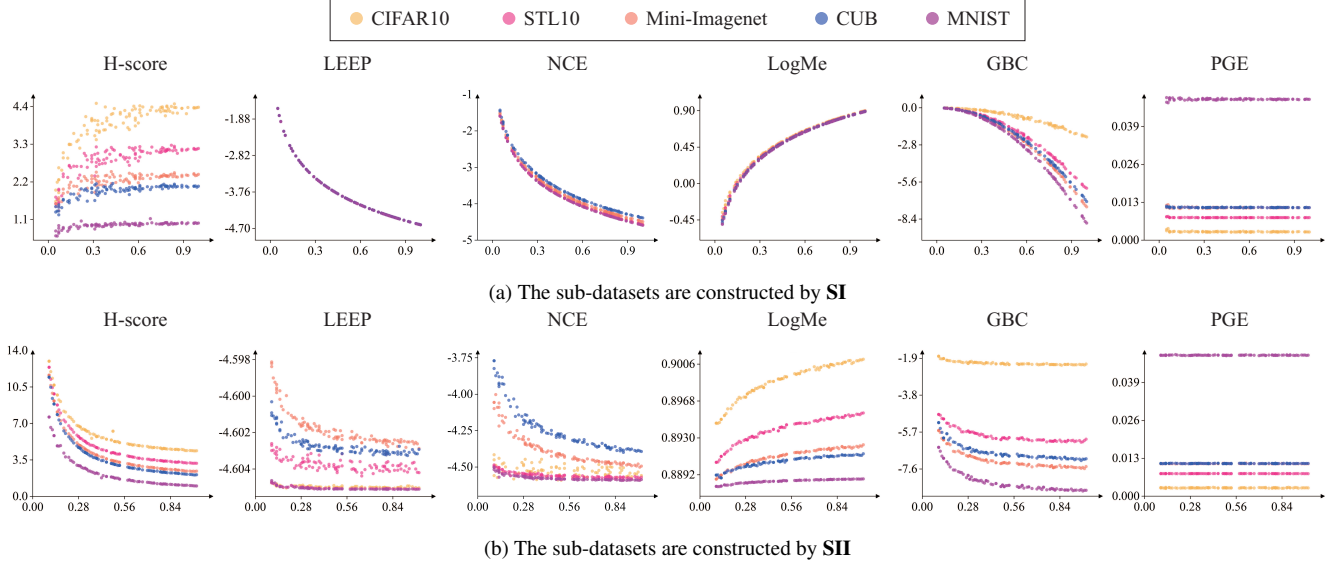


Figure 2. The stability comparison of different methods. The stability is indicated by the transfer score variation of different measure techniques along with increasing sampling ratio of each sub-dataset. The top row of the figure illustrates that we build target sub-datasets with strategy **SI** on CIFAR100. We compare the results with six existing transferability metrics. In each plot, the horizontal axis means the sampling ratio of each sub-dataset while the vertical axis is the transferability scores. The bottom row of the figure indicates that we construct sub-datasets with strategy **SII** on CIFAR100.

**SII:** The second approach randomly samples of a percentage between 10% and 100% images in each category.

We do not sample all target datasets with either of the two sampling approaches. Notably, we generate sub-datasets with **SI** when the number of samples in each category is small.

**Transfer Methods.** Previous studies have concentrated more on linear probing, we examine both fine-tuning and linear probing.

(1) *Linear Probing.* This approach freezes the feature extractor layer of the model and trains a task-related layer from scratch using the target dataset.

(2) *Fine-Tuning.* The model’s task-related layer is replaced by a new one, and then fine-tuned the entire model (the feature extractor and the task-related layer) on the target dataset.

**Others.** We run 600 epochs of linear probing and fine-tuning for each sub-target dataset (using SGD without Momentum and Cosine annealing [22] to adjust the learning rate with an initial learning rate of  $0.1 * \text{batchsize}/256$ ). Three classic backbones including Resnet18 [14], Resnet50 [14], and VGG16 [33] are adopted in the experiments.

## 4.2. Stability Comparison

In this section, we compare the proposed PGE and existing transferability measure techniques, including LEEP [24], LogMe [44], H-score [2], NCE [39] and GBC [26].

The CIFAR10, STL10, Mini-ImageNet, CUB, and MNIST are set as source datasets. CIFAR100 is set as the target dataset. What’s more, two sampling strategies **SI** and **SII** are adopted to evaluate the stability, as shown in Figure 2a and Figure 2b.

Figure 2 shows the transfer score variation of different measure techniques along with increasing sampling ratio of each sub-dataset. A stable measure technique should have an invariable score. From Figure 2a we can see that the curves of LEEP [24], LogMe [44], and NCE [39] almost overlap when randomly sampling categories over CIFAR100 as **SI**, which demonstrate that we can hardly discriminate what is best for the target dataset because they tend to yield similar transferability scores for all source datasets. As the sampling ratio increases, we observe that H-score [2] and LogMe [44] increase while LEEP, NCE, and GBC decrease. The proposed PGE shows remarkable superiority over these methods, as it produces stable and distinguishable results.

For the existing methods, the number of target dataset’s categories is an important parameter to compute the transferability scores. Therefore, the scores calculated by the existing method vary with the number of categories. Our calculation does not involve the number of categories. Hence, it is more stable than existing methods. We can get the correct result with only a portion of categories from the target dataset.

In Figure 2b, the sub-datasets are constructed by **SII**.

	CIFAR10 [18]		STL10 [5]		CIFAR100 [18]		CUB [41]		Aircraft [23]		Average Kendall's $\tau$
	LP	FT	LP	FT	LP	FT	LP	FT	LP	FT	
LEEP [24]	0.19	0	0	0	0	-0.6	0.19	0.2	-0.19	-0.19	-0.04
H-score [2]	<b>1</b>	<b>0.79</b>	<b>1</b>	<b>1</b>	<b>1</b>	0	-0.19	0.19	0.19	0.19	0.52
NCE [39]	0.39	0.19	-0.2	-0.2	0	-0.6	-0.19	-0.39	-0.79	-0.79	-0.26
LogMe [44]	<b>1</b>	<b>0.79</b>	<b>1</b>	<b>1</b>	<b>1</b>	0	-0.39	-0.4	-0.79	-0.4	0.281
GBC [26]	<b>1</b>	<b>0.79</b>	0.4	0.4	<b>1</b>	0	0.39	0.39	0.19	-0.19	0.44
<b>PGE (Ours)</b>	<b>1</b>	<b>0.79</b>	<b>1</b>	<b>1</b>	<b>1</b>	0	<b>0.39</b>	<b>0.39</b>	<b>0.79</b>	<b>0.39</b>	<b>0.68</b>

Table 2. The reliability comparison of different methods. The value (higher is better) indicates the correlation between the ranking calculated by the transferability estimation technique and the ranking of real transfer results. Overview of transferability results for selected source datasets in the image classification task. We describe the results for five target datasets with two transfer methods (Linear probing and Fine-tuning). The data in the Table are the correlations between the rankings (higher is better). Our proposed method obtains the highest Kendall's  $\tau$  [13] coefficient in most experiments and the highest average Kendall's  $\tau$  [13] coefficient for the different datasets.

	PGE Scores ( $10^{-2}$ )	LP(%)	FT(%)
CIFAR100	0.284	50.57	66.69
STL10	0.773	39.86	65.39
Mini-ImageNet	1.118	32.04	65.28
CUB	1.125	26.20	60.67
MNIST	4.842	17.32	62.66
		$\tau : 1$	$\tau : 0.79$

Table 3. The reliability of PGE scores and real transfer results obtained with two transfer methods Linear Probing (LP) and Fine-Tuning (FT).

LEEP [24] and NCE [39] yield distinguishable results, while the results are inconsistent with the transfer results. As the sampling ratio increases, we find that H-score, LEEP, NCE and GBC decrease while LogMe increases. We guess existing approaches may fail when the number of images is small. The distribution of features and labels of the few samples can not represent the true distribution. PGE uses the expected value of the principle gradient to calculate the transferability score. Using the expected value can effectively reduce the impact of abnormal gradients. Thus, the proposed PGE can still get the correct result. In summary, the proposed PGE yields more consistent and distinguishable results for both strategies. PGE obtained considerably varied transferability scores, which correspond with transfer outcomes.

### 4.3. Reliability Comparison

In this section, we adopt the consistence between the estimated score and the real transfer performance to compare the reliability of different methods. As mentioned in Section 3, the transferability score is supposed to correlate well with the final performance of a model after fine-tuning/linear probing on the target dataset. To validate the reliability of the proposed PGE, we conduct experiments with both fine-tuning and linear probing on CIFAR10, CI-

	PGE Scores ( $10^{-2}$ )	MIoU(%)
CIFAR100	3.86	65.09
CIFAR10	4.04	65.03
Mini-ImageNet	1.17	67.85
STL10	1.23	66.07
CUB	1.18	65.53
	$\tau : 0.79$	

Table 4. The generalizability of PGE with PASCAL VOC 2012 dataset as target dataset.

FAR100, STL10, CUB, and Aircraft. We chose five different source datasets for each target dataset. As shown in Table 2, the relevance between the transfer results and transferability score is computed with Kendall's  $\tau$  [13] coefficient. The proposed PGE achieves the highest average correlation 0.68 among all existing approaches. In the linear probing(LP) process, PGE identified the optimal source dataset for all five target datasets. In the fine-tuning process, PGE determines the optimal source for four target datasets. We achieved the highest results for CIFAR10, CUB, and Aircraft with fine-tuning and linear probing.

The results in Table 2 reveal that H-score and LogMe can produce competitive results on simple dataset (CIFAR10, STL10, and CIFAR100). However, most of existing approaches show poorly performance on more challenging dataset (CUB and Aircraft). We consider that existing methods are sensitive to the resolution of the images while the proposed PGE is robust enough to alleviate this issue.

Specifically, Table 3 presents the results of the estimated transferability scores and the transfer performance on target dataset CIFAR10. When linear probing(LP) is adopted, the transfer results completely match ( $\tau = 1$ ) the ranking of the PGE scores. For fine-tuning(FT), we also obtain the Kendall's  $\tau = 0.79$  and the top results and scores can be well-matched.

Pre-trained task	Transfer Target	H-score [2]	LEEP [24]	NCE [39]	GBC [26]	LogMe [44]	PGE (ours)
Classification	Classification	✓	✓	✓	✓	✓	✓
Classification	Regression	✗	✗	✗	✗	✓	✓
Unsupervised	Classification	✗	✗	✗	✗	✓	✓
Unsupervised	Regression	✗	✗	✗	✗	✓	✓

Table 5. Generalizability of different techniques for different transfer task. “✓ / ✗” indicates whether the technique is applicable / unapplicable for the current transfer task.

	Sup.	Uns. ( $10^{-2}$ )	LP (%)	FT (%)
Mini-ImageNet	4.35	5.00	48.21	61.83
CIFAR10	1.91	5.80	45.43	61.36
CIFAR100	2.56	7.79	45.34	59.47
CUB	4.75	7.81	37.93	55.82

Table 6. The ablation study on supervised (Sup.) and unsupervised (Uns.) pre-training strategy.

#### 4.4. Efficiency Comparison

Regarding a new source dataset, the existing methods need the pre-trained parameters trained on this dataset to measure the transferability, which is time-consuming. In contrast, our proposed method is more computational efficiency for the following reasons. First, by employing the gradient of the first-order optimization of the data directly, our method does not require any pre-training process for source datasets. Second, by analyzing the stability of the proposed method above, we can find that the proposed PGE can significantly reduce the computational cost by sub-sampling the dataset when computing the transferability distance score, which is not applicable in all other methods.

#### 4.5. Generalizability Comparison

We further extend our proposed PGE to cross-task adaptations. The source datasets are CIFAR10, CIFAR100, STL10, Mini-ImageNet, and CUB. The target dataset is PASCAL VOC 2012. The adaptation process aims to find a most suitable pre-trained model for segmentation task based on those classification datasets. The backbone here is VGG16 and epochs for pre-training is 100. The results are shown in Table 4. The values in Table 4 suggests us that models pre-trained on Mini-ImageNet may be a suitable initialization, which is verified by the segmentation accuracy.

We list four common transfer settings, as shown in Table 5. We can draw conclusions that all of the approaches can be easily adapted to classification tasks. When the source task and target task differs, H-score, LEEP, NCE, GBC can not estimate the transferability score. While our proposed PGE and LogMe are more practical to adapt to cross-task scenery. Nevertheless, LogMe estimates the maximum value of label evidence given features extracted

by pre-trained models. It models each target label as a linear model with Gaussian noise, and then optimizes the prior distribution parameters to obtain the average maximum (log) evidence of labels given the target sample embeddings. For classification and regression tasks, LogMe design different modules while our proposed PGE computes the transferability distance scores uniformly without pre-training.

#### 4.6. Ablation Study

Recent researches [16, 45] have shown that unsupervised techniques acquire more low- and mid-level information that is readily adaptable to a new domain than supervised cross-entropy models, which primarily learn high-level semantics in the last layers. In this subsection, we examine transferability distances in both cases as shown in Table 6. It has been experimentally found that supervised pre-training is more susceptible than unsupervised pre-training. A reasonable explanation for this is that category information is embedded into the backbone to improve discrimination but impair transferability.

### 5. Conclusion

Determining which source model is the most suitable guessing for a particular task is challenging. It is computationally costly to determine this by fine-tuning/linear probing all possible combinations of source models and target datasets. In this work, we start by summarizing the properties that a good transferability metric should possess. Building upon these assumptions, we propose a simple yet effective transferability estimation approach termed PGE based on principal gradient expectation. To properly evaluate the method’s validity, we applied two robust sub-sampling techniques on target data. The experimental results on both fine-tuning and linear probing demonstrate that our proposed PGE is superior to existing metrics. Since PGE computes the gradient of the backbone under unsupervised learning, it is more flexible and can be extended to different tasks depending on the task-related head layer to enable task agnostic in the future.



## References

- [1] Samira Abnar, Mostafa Dehghani, Behnam Neyshabur, and Hanie Sedghi. Exploring the limits of large scale pre-training. *arXiv preprint arXiv:2110.02095*, 2021. 2, 3
- [2] Yajie Bao, Yang Li, Shao-Lun Huang, Lin Zhang, Lizhong Zheng, Amir Zamir, and Leonidas Guibas. An information-theoretic approach to transferability in task transfer learning. In *2019 IEEE International Conference on Image Processing (ICIP)*, pages 2309–2313. IEEE, 2019. 2, 3, 6, 7, 8, 11
- [3] Tom Brown, Benjamin Mann, Nick Ryder, Melanie Subbiah, Jared D Kaplan, Prafulla Dhariwal, Arvind Neelakantan, Pranav Shyam, Girish Sastry, Amanda Askell, et al. Language models are few-shot learners. *Advances in neural information processing systems*, 33:1877–1901, 2020. 1
- [4] Xinlei Chen, Saining Xie, and Kaiming He. An empirical study of training self-supervised vision transformers. In *Proceedings of the IEEE/CVF International Conference on Computer Vision*, pages 9640–9649, 2021. 1
- [5] Adam Coates, Andrew Ng, and Honglak Lee. An analysis of single-layer networks in unsupervised feature learning. In *Proceedings of the fourteenth international conference on artificial intelligence and statistics*, pages 215–223. JMLR Workshop and Conference Proceedings, 2011. 2, 5, 7, 11
- [6] Ekin D Cubuk, Barret Zoph, Dandelion Mane, Vijay Vasudevan, and Quoc V Le. Autoaugment: Learning augmentation policies from data. *arXiv preprint arXiv:1805.09501*, 2018. 11
- [7] Li Deng. The mnist database of handwritten digit images for machine learning research [best of the web]. *IEEE signal processing magazine*, 29(6):141–142, 2012. 5, 11
- [8] Jacob Devlin, Ming-Wei Chang, Kenton Lee, and Kristina Toutanova. Bert: Pre-training of deep bidirectional transformers for language understanding. *arXiv preprint arXiv:1810.04805*, 2018. 1
- [9] Terrance DeVries and Graham W Taylor. Improved regularization of convolutional neural networks with cutout. *arXiv preprint arXiv:1708.04552*, 2017. 11
- [10] Josip Djolonga, Jessica Yung, Michael Tschannen, Rob Romijnders, Lucas Beyer, Alexander Kolesnikov, Joan Puigcerver, Matthias Minderer, Alexander D’Amour, Dan Moldovan, et al. On robustness and transferability of convolutional neural networks. In *Proceedings of the IEEE/CVF Conference on Computer Vision and Pattern Recognition*, pages 16458–16468, 2021. 3
- [11] Alexey Dosovitskiy, Lucas Beyer, Alexander Kolesnikov, Dirk Weissenborn, Xiaohua Zhai, Thomas Unterthiner, Mostafa Dehghani, Matthias Minderer, Georg Heigold, Sylvain Gelly, Jakob Uszkoreit, and Neil Houlsby. An image is worth 16x16 words: Transformers for image recognition at scale, 2020. 1
- [12] Mark Everingham, SM Eslami, Luc Van Gool, Christopher KI Williams, John Winn, and Andrew Zisserman. The pascal visual object classes challenge: A retrospective. *International journal of computer vision*, 111(1):98–136, 2015. 5
- [13] R Fagin, R Kumar, and D Sivakumar. Comparing top k lists. in proceedings of the fourteenth annual acm-siam symposium on discrete algorithms, soda’03, 2003. 5, 7, 11
- [14] Kaiming He, Xiangyu Zhang, Shaoqing Ren, and Jian Sun. Deep residual learning for image recognition. In *Proceedings of the IEEE conference on computer vision and pattern recognition*, pages 770–778, 2016. 1, 6
- [15] Jeremy Howard. Imagenette, 2019. URL <https://github.com/fastai/imagenette>, 2020. 11
- [16] Ashraf Islam, Chun-Fu Richard Chen, Rameswar Panda, Leonid Karlinsky, Richard Radke, and Rogerio Feris. A broad study on the transferability of visual representations with contrastive learning. In *Proceedings of the IEEE/CVF International Conference on Computer Vision*, pages 8845–8855, 2021. 2, 3, 8
- [17] Simon Kornblith, Jonathon Shlens, and Quoc V Le. Do better imagenet models transfer better? In *Proceedings of the IEEE/CVF conference on computer vision and pattern recognition*, pages 2661–2671, 2019. 3
- [18] Alex Krizhevsky, Geoffrey Hinton, et al. Learning multiple layers of features from tiny images. 2009. 2, 5, 7, 11
- [19] Ananya Kumar, Aditi Raghunathan, Robbie Jones, Tengyu Ma, and Percy Liang. Fine-tuning can distort pretrained features and underperform out-of-distribution. *arXiv preprint arXiv:2202.10054*, 2022. 2
- [20] Ze Liu, Han Hu, Yutong Lin, Zhuliang Yao, Zhenda Xie, Yixuan Wei, Jia Ning, Yue Cao, Zheng Zhang, Li Dong, Furu Wei, and Baining Guo. Swin transformer v2: Scaling up capacity and resolution. In *International Conference on Computer Vision and Pattern Recognition (CVPR)*, 2022. 1
- [21] Ze Liu, Yutong Lin, Yue Cao, Han Hu, Yixuan Wei, Zheng Zhang, Stephen Lin, and Baining Guo. Swin transformer: Hierarchical vision transformer using shifted windows. In *Proceedings of the IEEE/CVF International Conference on Computer Vision (ICCV)*, 2021. 1, 11
- [22] Ilya Loshchilov and Frank Hutter. Sgdr: Stochastic gradient descent with warm restarts. *arXiv preprint arXiv:1608.03983*, 2016. 6
- [23] Subhransu Maji, Esa Rahtu, Juho Kannala, Matthew Blaschko, and Andrea Vedaldi. Fine-grained visual classification of aircraft. *arXiv preprint arXiv:1306.5151*, 2013. 5, 7, 11
- [24] Cuong Nguyen, Tal Hassner, Matthias Seeger, and Cedric Archambeau. Leep: A new measure to evaluate transferability of learned representations. In *International Conference on Machine Learning*, pages 7294–7305. PMLR, 2020. 2, 3, 6, 7, 8, 11
- [25] Maria-Elena Nilsback and Andrew Zisserman. Automated flower classification over a large number of classes. In *2008 Sixth Indian Conference on Computer Vision, Graphics & Image Processing*, pages 722–729. IEEE, 2008. 11
- [26] Michal Pándy, Andrea Agostinelli, Jasper Uijlings, Vittorio Ferrari, and Thomas Mensink. Transferability estimation using bhattacharyya class separability. In *Proceedings of the IEEE/CVF Conference on Computer Vision and Pattern Recognition*, pages 9172–9182, 2022. 2, 3, 6, 7, 8, 11
- [27] Omkar M Parkhi, Andrea Vedaldi, Andrew Zisserman, and CV Jawahar. Cats and dogs. In *2012 IEEE conference on computer vision and pattern recognition*, pages 3498–3505. IEEE, 2012. 11

- [28] Alec Radford, Jong Wook Kim, Chris Hallacy, Aditya Ramesh, Gabriel Goh, Sandhini Agarwal, Girish Sastry, Amanda Askell, Pamela Mishkin, Jack Clark, et al. Learning transferable visual models from natural language supervision. In *International Conference on Machine Learning*, pages 8748–8763. PMLR, 2021. 1
- [29] Aditya Ramesh, Prafulla Dhariwal, Alex Nichol, Casey Chu, and Mark Chen. Hierarchical text-conditional image generation with clip latents. *arXiv preprint arXiv:2204.06125*, 2022. 1
- [30] Cedric Renggli, André Susano Pinto, Luka Rimanic, Joan Puigcerver, Carlos Riquelme, Ce Zhang, and Mario Lučić. Which model to transfer? finding the needle in the growing haystack. In *Proceedings of the IEEE/CVF Conference on Computer Vision and Pattern Recognition*, pages 9205–9214, 2022. 2
- [31] Olga Russakovsky, Jia Deng, Hao Su, Jonathan Krause, Sanjeev Satheesh, Sean Ma, Zhiheng Huang, Andrej Karpathy, Aditya Khosla, Michael Bernstein, et al. Imagenet large scale visual recognition challenge. *International journal of computer vision*, 115(3):211–252, 2015. 1, 2
- [32] Chitwan Saharia, William Chan, Saurabh Saxena, Lala Li, Jay Whang, Emily Denton, Seyed Kamyar Seyed Ghasemipour, Burcu Karagol Ayan, S Sara Mahdavi, Rapha Gontijo Lopes, et al. Photorealistic text-to-image diffusion models with deep language understanding. *arXiv preprint arXiv:2205.11487*, 2022. 1
- [33] Karen Simonyan and Andrew Zisserman. Very deep convolutional networks for large-scale image recognition. *arXiv preprint arXiv:1409.1556*, 2014. 6
- [34] Jie Song, Yixin Chen, Xinchao Wang, Chengchao Shen, and Mingli Song. Deep model transferability from attribution maps. *Advances in Neural Information Processing Systems*, 32, 2019. 1
- [35] Jie Song, Yixin Chen, Jingwen Ye, Xinchao Wang, Chengchao Shen, Feng Mao, and Mingli Song. Depara: Deep attribution graph for deep knowledge transferability. In *Proceedings of the IEEE/CVF Conference on Computer Vision and Pattern Recognition*, pages 3922–3930, 2020. 1
- [36] J Michael Steele. *The Cauchy-Schwarz master class: an introduction to the art of mathematical inequalities*. Cambridge University Press, 2004. 2, 4
- [37] Yang Tan, Yang Li, and Shao-Lun Huang. Otce: A transferability metric for cross-domain cross-task representations. In *Proceedings of the IEEE/CVF Conference on Computer Vision and Pattern Recognition*, pages 15779–15788, 2021. 2
- [38] Lisa Torrey and Jude Shavlik. Transfer learning. In *Handbook of research on machine learning applications and trends: algorithms, methods, and techniques*, pages 242–264. IGI global, 2010. 2
- [39] Anh T Tran, Cuong V Nguyen, and Tal Hassner. Transferability and hardness of supervised classification tasks. In *Proceedings of the IEEE/CVF International Conference on Computer Vision*, pages 1395–1405, 2019. 2, 3, 6, 7, 8, 11
- [40] Oriol Vinyals, Charles Blundell, Timothy Lillicrap, Daan Wierstra, et al. Matching networks for one shot learning. *Advances in neural information processing systems*, 29, 2016. 2, 5, 11
- [41] Catherine Wah, Steve Branson, Peter Welinder, Pietro Perona, and Serge Belongie. The caltech-ucsd birds-200-2011 dataset. 2011. 2, 5, 7, 11
- [42] Pengfei Wei, Thanh Vinh Vo, Xinghua Qu, Yew Soon Ong, and Zejun Ma. Transfer kernel learning for multi-source transfer gaussian process regression. *IEEE Transactions on Pattern Analysis and Machine Intelligence*, 2022. 2
- [43] LI Xuhong, Yves Grandvalet, and Franck Davoine. Explicit inductive bias for transfer learning with convolutional networks. In *International Conference on Machine Learning*, pages 2825–2834. PMLR, 2018. 2
- [44] Kaichao You, Yong Liu, Jianmin Wang, and Mingsheng Long. Logme: Practical assessment of pre-trained models for transfer learning. In *International Conference on Machine Learning*, pages 12133–12143. PMLR, 2021. 2, 3, 6, 7, 8, 11
- [45] Nanxuan Zhao, Zhirong Wu, Rynson WH Lau, and Stephen Lin. What makes instance discrimination good for transfer learning? *arXiv preprint arXiv:2006.06606*, 2020. 2, 3, 8

The supplementary materials provide more details about the model architecture, experimental setup, and additional results.

## A. Model Architectures

Recall that we decouple the model architecture into feature extractor (backbone)  $w$  and task-related head layer  $h$ . For a fair comparison, each group of trials adopted the same backbone. For classification tasks, we examine the effectiveness of the proposed PGE on both ResNet18 and ResNet50. For cross-task (from classification to segmentation) validation, the VGG16 is utilized as the backbone. Besides, we also conduct experiments on vision transformers [21] to showcase the flexibility of our proposed method. Table ?? presents the results of Swin Transformer (v1).

## B. Experimental Setup

**Dataset.** We conduct additional experiments on the following classification datasets: CIFAR10 [18], CIFAR100 [18], STL10 [5], Mini-ImageNet [40], CUB [41], MNIST [7], FGVC-Aircraft(Aircraft) [23], Flowers [25], Imagenette [15], Pets [27]. The information, including the resolution size (Resolution), image number (Img), and class number (Class) of above datasets are summarized in Table 7.

Dataset	Resolution	Img	Class
CIFAR10 [18]	$32 \times 32$	60k	10
CIFAR100 [18]	$32 \times 32$	60k	100
STL10 [5]	$96 \times 96$	13k	10
Mini-ImageNet [40]	$84 \times 84$	60k	200
CUB [41]	$512 \times 512$	11.7k	200
MNIST [7]	$28 \times 28$	70k	10
Aircraft [23]	$512 \times 512$	10k	100
Flowers [25]	$512 \times 512$	8.1k	102
Imagenette [15]	$512 \times 512$	13.4k	10
Pets [27]	$512 \times 512$	7.3k	10

Table 7. The summary information of datasets used in the supplementary material.

**Evaluation.** To ensure the correctness of the subsequent description, we will once again describe two distinct robust subsampling techniques as follows:

**SI:** The first approach randomly samples 5% to 100% of the target categories and uses all images in these categories.

**SII:** The second approach randomly samples of a percentage between 10% and 100% images in each category.

**Transfer Methods.** Previous studies have concentrated more on linear probing, we examine both fine-tuning and linear probing.

(1) *Linear Probing.* This approach freezes the feature extractor layer of the model and trains a task-related layer from scratch using the target dataset.

(2) *Fine-Tuning.* The model’s task-related layer is replaced by a new one, and then fine-tuned the entire model (the feature extractor and the task-related layer) on the target dataset.

**Data Augmentation Strategy** Different data augmentation methods are applied on different datasets. The images in CIFAR10, CIFAR100 and STL10 are augmented by random horizontal flip, AutoAugment(CIFAR10 Policy) [6], Cutout [9] and normalization operation. Only normalization is applied on MNIST because images in this dataset are black-and-white. The images in the other datasets are augmented by random horizontal flip, AutoAugment(ImageNet Policy) and normalization operation.

**Kendall’s coefficient** [13] Kendall’s  $\tau$  coefficient is a measure of rank correlation: the similarity of the orderings of the data when ranked by each of the quantities. Kendall’s  $\tau$  coefficient is defined as:

$$\tau = \frac{2}{n(n-1)} \sum_{i < j} \text{sgn}(x_i - x_j) \text{sgn}(y_i - y_j) \quad (15)$$

$\mathcal{X}$  and  $\mathcal{Y}$  represent two rankings respectively. In Equation 15,  $x_i \in \mathcal{X}$ ,  $y_i \in \mathcal{Y}$ ,  $n$  indicates the number of items in the ranking. The  $\text{sgn}(\cdot)$  function is a symbolic function.

## C. Additional Results

### C.1. Stability Comparison

The scores obtained from LEEP [24], NCE [39], and LogMe [44] vary with the sampling ratio. In Figure 3a and Figure 3b, the sub-datasets are constructed by SI based on CIFAR10 and STL10, respectively. As the sampling ratio increases, we observe that the scores of LEEP, NCE, LogMe, and GBC [26] decline, while the results of H-score is stable. Besides, the results of H-score [2], LEEP, NCE and LogMe can hardly be distinguished. It turns out that those methods failed in this circumstance. While GBC produces discriminative scores when the sampling ratio is high. As for our results, PGE can still obtain promising transferability distance scores. In Figure 3c and Figure 3d, the

Source	PGE Scores	FT Results
<b>Food</b>	<b>0.188</b>	<b>44.69</b>
Flowers	0.190	22.73
Imagenette	0.202	25.79
Pets	0.205	27.63
Aircraft	0.237	17.50
		$\tau : 0.39$

Table 8. The reliability of PGE scores and real transfer results with swin transformer(v1).

sub-datasets are generated based on sampling ratio in each category based on SII. When the sampling ratio is low, it

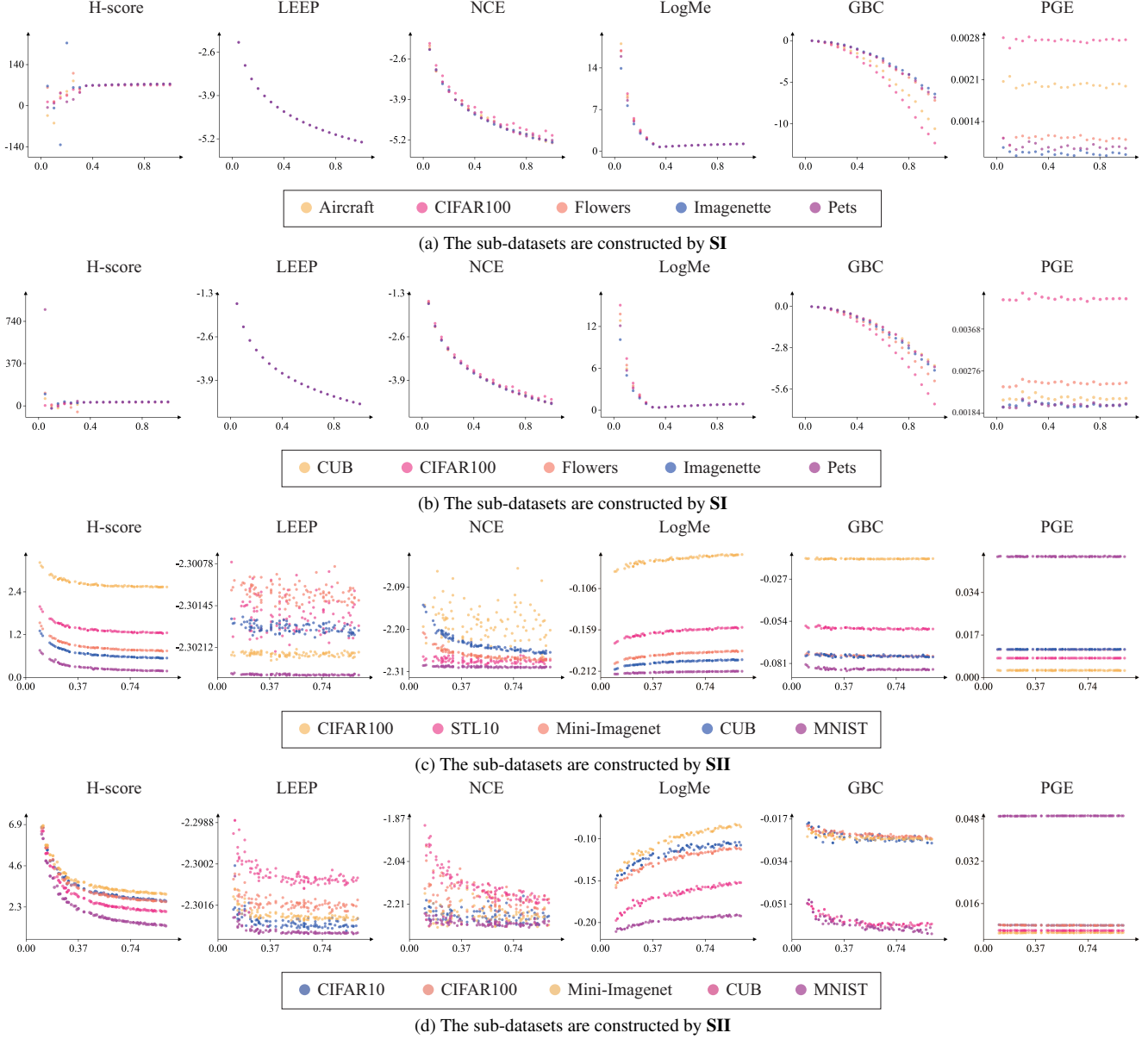


Figure 3. The stability comparison of different methods. The stability is indicated by the transfer score variation of different measure techniques along with increasing the sampling ratio of each sub-dataset. The four rows in the figure represent illustrate that we build target sub-datasets on CIFAR10, STL10, CUB, and Aircraft, respectively. We compare the results with six existing transferability metrics. In each plot, the horizontal axis means the sampling ratio of each sub-dataset, while the vertical axis is the transferability scores.

is also difficult to distinguish the GBC scores of different source datasets. When CUB and Aircraft are used as target datasets, H-score, LEEP, NCE, and LogMe all deteriorate. Our method for estimating transferability is based on principal gradient expectation, which can reduce the effect of odd gradients. The number of categories in the target dataset is not used to compute the PGE score. So the results of our method are always stable and distinguishable under various conditions.

## C.2. Reliability Comparison

We present more detailed results on estimated scores and real transfer performance. We selected four target datasets, which are CIFAR100, STL10, CUB, and Aircraft. When CIFAR100 is used as the target dataset, we show the results with **SI** and **SII**. Specifically, Table 9 presents the results of the estimated transferability scores and the transfer performance on target datasets. In addition, the table shows the relevance between the transfer results and the transferability

Target	Source	PGE Scores( $10^{-2}$ )	LP Results	FT Results
CIFAR100(SI)	CIFAR10	0.289	28.64	59.09
	STL10	0.775	27.05	57.96
	Mini-Imagenet	1.117	23.15	58.81
	CUB	1.123	17.84	55.98
	MNIST	4.838	9.20	59.14
			$\tau : 1$	$\tau : 0$
CIFAR100(SII)	CIFAR10	0.285	16.98	42.77
	STL10	0.774	16.63	41.03
	Mini-Imagenet	1.117	13.71	42.01
	CUB	1.121	9.63	38.62
	MNIST	4.839	4.10	42.13
			$\tau : 1$	$\tau : 0.2$
STL10	Mini-Imagenet	0.500	48.21	61.83
	CIFAR10	0.580	45.43	61.36
	CIFAR100	0.779	45.34	59.47
	CUB	0.781	37.93	55.82
	MNIST	4.920	21.55	52.58
			$\tau : 1$	$\tau : 1$
CUB	Imagenette	0.087	13.55	124.89
	Pets	0.098	13.28	126.21
	Flowers	0.112	13.24	126.06
	Aircraft	0.202	38.70	119.63
	Cifar100	0.276	10.93	120.23
			$\tau : 0.4$	$\tau : 0.4$
Aircraft	Imagenette	2.036	67.74	60.59
	Pets	2.041	66.39	58.33
	CUB	2.162	60.15	50.24
	Flowers	2.506	66.19	60.35
	Cifar100	4.345	54.63	57.65
			$\tau : 0.79$	$\tau : 0.39$

Table 9. The reliability of PGE scores and real transfer results.

score.

Swin transformer(v1) are employed as the architecture to conduct another experiment. CUB is set as the target dataset and Food, Flowers, Imagenette, Pets, and Aircraft are set as source datasets for this experiment. The LP results are low and similar, which we believe is caused by the structure of the transformer. The FT results are shown in Table 8, PGE selects the optimal source dataset for the target dataset.